J. Fluid Mech. (1978), *vol.* 86, *part* 1, *pp.* 15–32
Printed in Great Britain

Shock waves at a fast–slow gas interface

By A. M. ABD-EL-FATTAH AND L. F. HENDERSON
Department of Mechanical Engineering, University of Sydney,
New South Wales 2006, Australia

(Received 13 June 1977 and in revised form 12 September 1977)

This paper presents the results of experiments on plane shock waves refracting at air/SF_6 and He/CO_2 interfaces. These are called fast–slow gas combinations because the speed of sound in the incident shock gas is greater than that in the transmitting shock gas. Our work was based on a generalization of the von Neumann (1943) classification of shocks into two classes called weak and strong. We introduced two subclasses of each of these, giving in all four groups of phenomena for study. This is possibly an exhaustive list, at least for conditions where the gases are approximately perfect. We present data on all four groups and study various transition conditions both within and across the groups. Our results appear to conflict with a previously reported irregular refraction; in fact we could apparently completely suppress this wave system by attention to our gas purity and boundary conditions. In its place we found a different system which appears to be a new phenomenon. We found another new system which has the appearance of a Mach-reflexion type of refraction but with its shock dispersed into a band of wavelets. It is interesting that the wavelets remain intense enough to induce identifiable vortex sheets in the flow. Finally we found yet another refraction of the Mach-reflexion type which had no detectable vortex sheet emanating from the triple point: such a system was foreshadowed by von Neumann.

1. Introduction

In an earlier paper (Abd-El-Fattah, Henderson & Lozzi 1976) we presented the results of our experiments on shock waves refracting at a CO_2/He interface. The experimental technique was described fully in that paper, but briefly the gases were initially prevented from mixing by a delicate membrane about 5×10^{-8} m (or roughly 10 molecules) thick then a plane shock i was started in the CO_2 and refracted as it tore through the membrane and entered the He. The refraction was called slow–fast because the speed of sound a_{CO_2} in the incident gas was less than that in the transmitting gas: $a_{CO_2} < a_{He}$. The phenomena which we observed depended on the angle of incidence ω_0 which i made with the gas interface. When ω_0 was comparatively small, i.e. when there was nearly head-on incidence, we obtained a regular refraction with a reflected expansion wave e, but with steadily increasing ω_0 we obtained successively two different irregular refractions, the first of which was distinguished by the fact that its transmitted shock t was a bound precursor wave, while for the second t was a free precursor. The experiments showed that all the wave systems were closely self-similar. A simple piston theory of the phenomena was found to be in good agreement with the data.

In this paper we present experimental data on the reciprocal group of phenomena

which occur during fast–slow refraction. We used two gas combinations, namely He/CO_2 and air/SF_6. They were chosen both for their disparate physical properties and for convenience in obtaining conditions where shock polar theory indicated that previously unobserved phenomena were to be found (Henderson 1966). The structural or topological properties of the polar diagram are also the basis for a convenient classification of the phenomena. This was first done by von Neumann (1943) for shock *reflexion*. He recognized weak and strong incident shocks and the fact that they were associated with different reflexion phenomena. Much later Kawamura & Saito (1956) arrived at the same conclusion independently. Von Neumann defined the limiting condition separating the two types in terms of a polynomial equation of eighth degree in which the variable was the Mach number downstream of i. In view of the pioneering experiments of Jahn (1956) it will be worthwhile to make further subdivisions. The weak incident shock group will be split into two further groups called the 'very weak' and the 'weak' incident shock groups, while the strong one will be split into the 'strong' and the 'stronger' incident shock groups. In general each of these groups is associated with a different physical phenomenon. We consider each one in turn, but the emphasis will be on the irregular wave systems.

2. The very weak incident shock group

A representative series of events corresponding to our experiments with this group is shown† in figure 1. The incident shock i was in air and the transmitted shock t in SF_6; the speed of sound ratio (air/SF_6) was 2·54. If P is the pressure then the inverse shock strength is defined by $\xi_i \equiv P_0/P_1$, where the subscripts are illustrated in the diagram. For this series ξ_i was held constant at $\xi_i = 0{\cdot}909$ ($\xi_i^{-1} = 1{\cdot}10$). In figure 1 (*a*), $\omega_0 = 50°$ and we obtained a regular refraction with a reflected shock, which we denote by *RRR*. The polar diagram provides two solutions marked α_1 and α_2, but it was the weaker α_1 solution which always appeared in the experiments. It was shown in Henderson (1966) and earlier by Taub (1947) that the theory of *RRR* could be reduced to a polynomial equation of degree 12 and a discussion was given on which of its roots were physically meaningful. In the present case‡ only $\alpha_{1,2}$ are in this category. From this equation we can calculate the wave angles ω_r and ω_t of the reflected and transmitted shocks r and t respectively and compare these with the measured values. The results are shown in figure 2 and the agreement is good. Similar calculations on *RRR* have been made by Polachek & Seeger (1951) and Taub (1951) for other gas combinations.

If ω_0 is increased to $\omega_0 = 63{\cdot}24°$ as in figure 1 (*b*), then α_1 coincides with the polar intersection point A_1, but this also requires i to map into the same point. The physical consequences are that r degenerates to a Mach line and the shock impedances of the two gases become equal. If ω_0 is again increased to say 68·00° (figure 1 *c*) then we also get a regular refraction but now its reflected wave is an expansion e; and we denote it by *RRE*. Theory and experiment are in good agreement: see figure 2. Clearly the transition condition for $RRR \leftrightarrow RRE$ is at the coincidence $\alpha_1 \equiv e_1 \equiv A_1$. These wave systems are well known and schlieren photographs of them will be omitted.

† Sometimes the polar diagram is plotted in terms of P/P_0 and at other times in terms of $\ln P/P_0$, the choice being made for convenience in displaying the polar geometry.

‡ The symbolism was developed in Henderson (1966).

The next event of interest occurs at $\omega_0 = 74{\cdot}81°$ (figure 1*d*), and here the free-stream Mach number M_1 ahead of the leading expansion wave is such that $M_1 = 1$, so i must now coincide with the sonic point S_1 on the air polar $i \equiv S_1$. When $\omega_0 > 74{\cdot}81$, we have $M_1 < 1$ and this implies the existence of an irregular refraction (figure 1*e*; figures 3 and 4, plate 1). We shall call this system a centred-expansion irregular refraction *CER*. The transition condition for $RRE \leftrightarrow CER$ is evidently $i \equiv S_1$, where $M_1 = 1$.

We spent some time experimenting with the *CER* system, and one of our earliest photographs of it is shown in figure 3. In this example i is curved concave backwards and we concluded by comparison of polar diagrams that it is of the same type as one obtained by Jahn during his experiments with an air/CO_2 interface with $\xi_i = 0{\cdot}85$. We were surprised to find that i had the same sort of curvature even in regular refraction. Eventually we traced this to the fact that our membranes were leaking slightly, and in particular the SF_6 diffused into the air and set up a continuous gradient in the speed of sound along the normal to the interface. Now if we define the free-stream Mach number M_0 of i as $M_0 = M_i/\sin\omega_0$, where M_i is the shock Mach number, then M_0 becomes larger as i approaches the interface and this is what causes i to curve and to emit a band of expansion waves. We then stacked four membranes onto the wire frame and thereafter there was no sign of this for either the *RRR* or the *RRE* system, but the effect persisted in a modified form in the irregular range. By a variety of other experiments we finally traced the effect to disturbances caused by the gap between the front and the back plates (figure 1*e*). This gap is needed to accommodate the wire frame which holds the membranes. In figure 3 the gap is about 2 cm wide but in figure 4 it has been reduced to about 2 mm by modifying the apparatus. Otherwise both experiments were done under the same conditions with $\omega_0 \approx 80°$. It will be noticed that, while i is markedly curved in figure 3, it is practically straight in figure 4. So we concluded† that in our experiments the curved-i irregular refraction could be modified or even suppressed by eliminating membrane leakage and an excessive gap width. The *CER* system shown in figure 4 is largely free of these effects and should be the truly fundamental system. The gap still has some effect because a small amount of gas passes through it and generates a weak expansion wave called the corner signal *CS*. It travels everywhere at the local speed of sound and it is a simple matter to calculate the trajectory angle χ (figure 1*e*) of the point where the signal first catches up with i. From the geometry of the system χ is given by

$$\sin\chi = \sin\omega_0 \frac{[a_1^2 - (V_i - V_{pi})^2]^{\frac{1}{2}} - V_i \cot\omega_0}{[a_1^2 - (V_i - V_{pi})^2 + V_i^2]^{\frac{1}{2}}}, \tag{1}$$

where V_i is the velocity of i normal to itself and V_{pi} the corresponding piston velocity. These quantities are related by the well-known equation

$$V_{pi} = \frac{2}{\gamma+1}\frac{V_i^2 - a_0^2}{V_i}, \tag{2}$$

where γ is the ratio of specific heats and $a_{0,1}$ are the speeds of sound ahead of and behind i. For the experiment in figure 4 we get $\chi = 5{\cdot}3°$ and faint signs of the corner signal intersecting i at this angle can be seen on the original of the photograph, but this produces negligible curvature of i.

† Our experiments seem to conflict with those of Jahn here. We understand that the gap was very small in his apparatus, and there seems to be no sign of gas leakage in his interferograms.

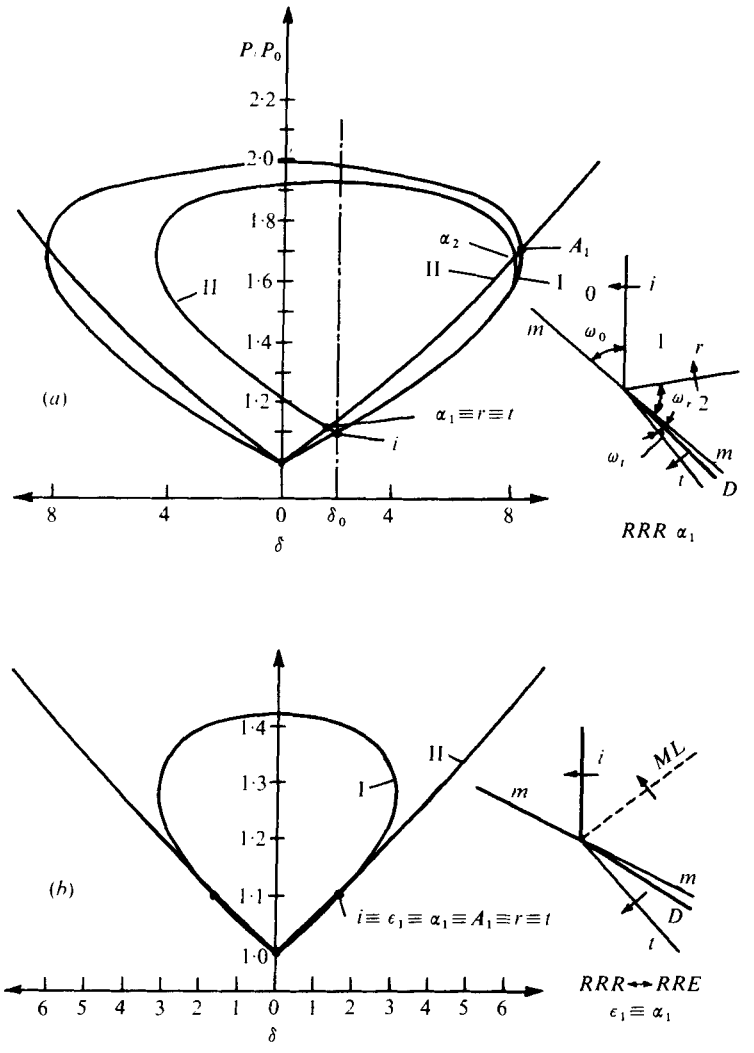

FIGURES 1 (*a*), (*b*). For legend see facing page.

Thus the curvature of i is possibly not a truly fundamental effect, and if so the explanation given by Henderson (1966) is wrong. Actually the polar diagram shown in figure 14 of that paper is still correct if the characteristics shown there are thought of as being caused by the continuous interaction of i with air contaminated by CO_2. When the contamination and other boundary effects are negligible, so that, as in our experiments although not in Jahn's, i becomes practically straight, then the polar diagram has the form shown in figure 1(*e*) of the present paper, although now of course it is constructed for air/SF_6. It will be noticed that i maps into the segment iS_1, which implies that the pressure and streamline direction are changing for at least part of the flow immediately downstream of i. The only way for this to be compatible with a straight shock in the physical plane is for i to have a singular point at the interface where all the variation occurs. Evidence for this is provided by the fact that none of the wave systems has a length scale; they are all in fact self-similar. We used these

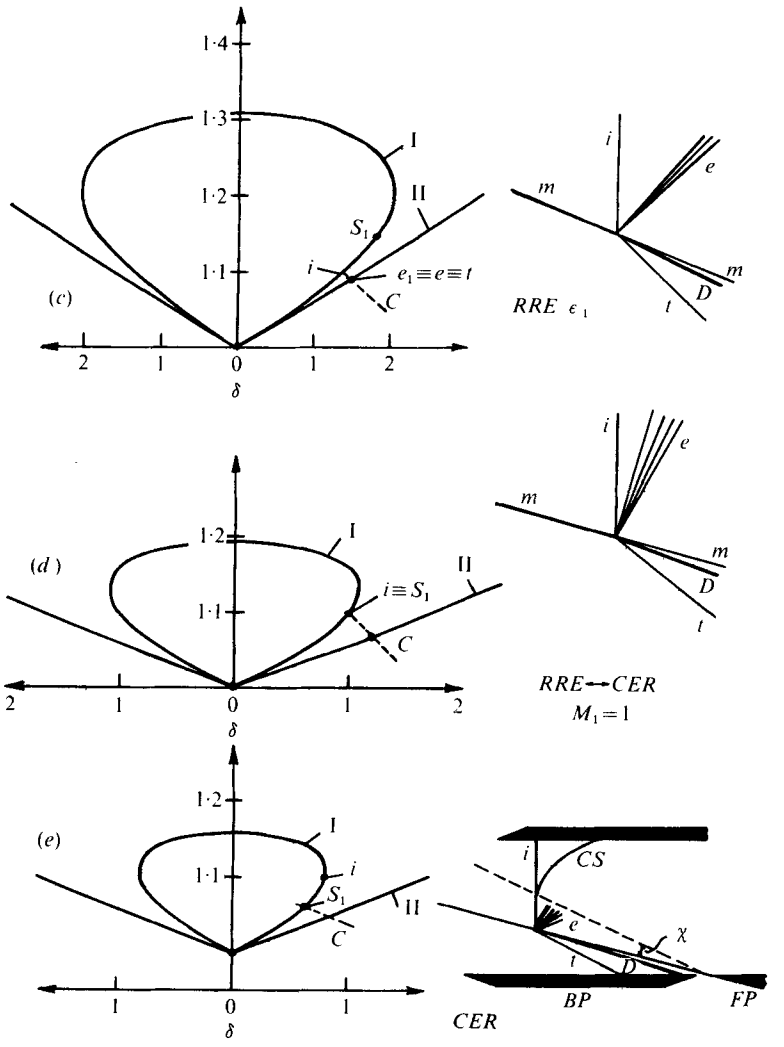

FIGURE 1. Polar diagrams for the refraction of a plane shock in the very weak incident shock group ($\xi_i = 0{\cdot}909$) at an air/SF_6 interface. (*a*) Regular refraction with a reflected shock *RRR* at $\omega_0 = 50°$. (*b*) Transition condition defined by $i \equiv A_1 \equiv \epsilon_1 \equiv \alpha_1 \equiv r \equiv t$ for $RRR \leftrightarrow RRE$, at $\omega_0 = 63{\cdot}24°$. (*c*) Regular refraction with a reflected expansion *RRE* at $\omega_0 = 68{\cdot}00°$. (*d*) Transition condition defined by $i \equiv S_1$ or $M_1 = 1$, for $RRE \leftrightarrow CER$ at $\omega_0 = 74{\cdot}81°$. (*e*) Centred-expansion irregular refraction at $\omega_0 = 78{\cdot}00°$. *i*, incident shock; *r*, reflected shock; *e*, reflected expansion wave; *t*, transmitted shock; *P*, pressure; δ, streamline deflexion; *m*, gas interface; *D*, deflected gas interface; *M*, Mach number; $\alpha_{1,2}$, physically realistic roots of the polynomial solution equation for *RRR*; ϵ_1, solution for *RRE*; A_1, intersection point between the primary polars for air and SF_6; S_1, sonic point on the air polar; ω_0, ω_r, ω_t, wave angles of incident, reflected and transmitted shocks respectively; I, II, primary polars for air and SF_6 respectively; III, reflected shock polar; *C*, characteristic; *FP*, front plate; *BP*, back plate; *CS*, corner signal.

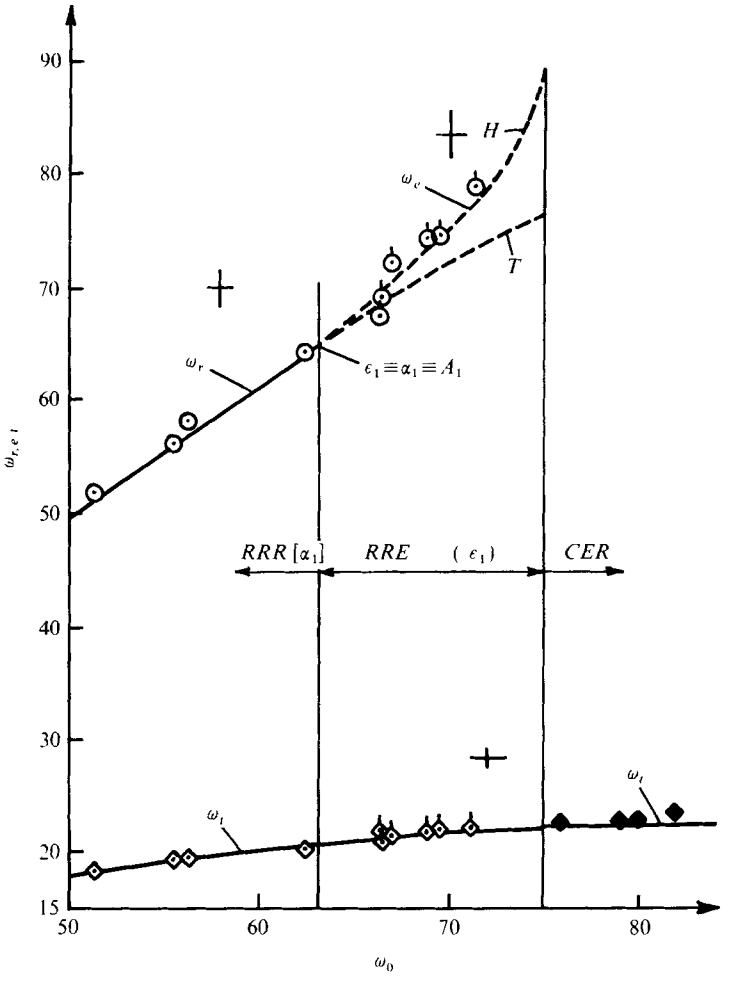

FIGURE 2. Comparison of the theoretically and experimentally determined wave angles from the refraction of a plane shock in the very weak group ($\xi_i = 0{\cdot}909$) at an air/SF_6 interface. ○, ◇, *RRR* experimental data for the reflected and transmitted shock wave angles compared with the α_1 solution; ○, ◇, *RRE* experimental data for the reflected and transmitted shock wave angles compared with the ϵ_1 solution; ◆, *CER* experimental data for the transmitted shock; +, magnitude of experimental error; *H*, *T*, head and tail of the reflected expansion wave respectively. For other symbols see caption to figure 1.

ideas to calculate ω_t at the interface for the *CER* system and the results are compared with the data in figure 2; the agreement is good. It is also possible to compute the head and tail wave angles of the reflected expansion but such waves are so weak that they are poorly defined in the schlieren photographs, so our measurements of them were too inaccurate to be of value. At the transition $RRE \leftrightarrow CER$, we have $M_1 = 1$, i.e. $\omega_0 = \omega_0(S_1)$, so the head wave of the expansion is normal to the oncoming flow, but for the irregular range $\omega_0 > \omega_0(S_1) = 74{\cdot}81°$ the wave must lean forward in the flow. This is possible because the flow is unsteady and $M_1 < 1$.

3. The weak incident shock group

The sequence of events which we studied as an example of this group is illustrated in figure 5. It was convenient to use an He/CO_2 interface because the polars and phenomena were then distinct enough to give decisive results; ξ_i was held constant at $\xi_i = 0{\cdot}66\dot{6}$ ($\xi_i^{-1} = 1{\cdot}5$). With $\omega_0 = 55°$ we obtained a regular refraction with a reflected shock RRR (figure 5*a*). There were two roots $\alpha_{1,2}$ which were physically acceptable but it was the weaker root α_1 which appeared in the shock tube. Agreement between theory and experiment is good; see figure 6. A double root ($\alpha_1 \equiv \alpha_2$) forms when ω_0 is increased to $\omega_0 = 57{\cdot}40°$ (figure 5*b*) but for larger ω_0 the roots become complex (figure 5*c*). This implies transition to an irregular refraction, and in Henderson (1966) this was referred to as 'an unknown irregular refraction'. We found it to be a refraction of the Mach-reflexion type MRR (figure 7, plate 2).

We experimented with the transition condition for $RRR \leftrightarrow MRR$ and, as near as we could determine, it was given by the double-root condition $\alpha_1 \equiv \alpha_2$. It is important to note that this point occurs at a smaller pressure ordinate than that for the intersection point A_1 of the primary He and CO_2 polars. We denote this property by ord $(\alpha_1 \equiv \alpha_2) <$ ord A_1. *Actually, by a generalization of the von Neumann classification it is this property which defines the weak incident shock groups.* Conversely, the strong groups are those for which ord $(\alpha_1 \equiv \alpha_2) >$ ord A_1 (figure 8*c*) and the limiting condition separating them is evidently ord $(\alpha_1 \equiv \alpha_2) =$ ord A_1. For shock *reflexion* off a rigid surface the double-root point $\alpha_1 \equiv \alpha_2$ is on the ordinate axis, and it is remarkable that this condition for weak shock reflexion does *not* predict transition to Mach reflexion $RR \leftrightarrow MR$ (Smith 1945; Bleakney & Taub 1949; Kawamura & Saito 1956; Henderson & Lozzi 1975) yet *does* predict correctly the refraction transition $RRR \leftrightarrow MRR$ (figure 6). Presumably this criterion would eventually fail if the shock impedance of the transmitting medium were to become large enough, for if we imagined that the impedance of this gas was increased without limit then we should convert the refraction to a reflexion.

After transition to MRR the reflected shock r is part of a Mach reflexion, but the well-known three-shock theory fails to provide any physically acceptable solutions for a weak system. Therefore we have had to be content with comparing our experimental data with the theoretical values of ω_r at transition, and similarly for ω_t and the deflexion angle of the gas interface ω_d. The MRR system shown in figure 7 has an interesting property foreshadowed by von Neumann, namely the absence of a contact discontinuity (vortex sheet) arising from the three-wave confluence point of the Mach reflexion. This must be due to the entropy difference between the flow downstream of r and the Mach stem n becoming too small to induce a detectable vortex sheet. Of course it is well known that the entropy change for weak shocks is only a third-order effect of the streamline deflexion (Landau & Lifshitz 1959, p. 323). If ω_0 is now increased to $\omega_0 = 64{\cdot}65°$, then $M_1 = 1$ and r degenerates to a Mach line. For larger ω_0 the Mach reflexion can no longer exist and there must be a further transition to another, irregular refraction, but we shall defer discussion of this until the next section, where it can be displayed more definitely.

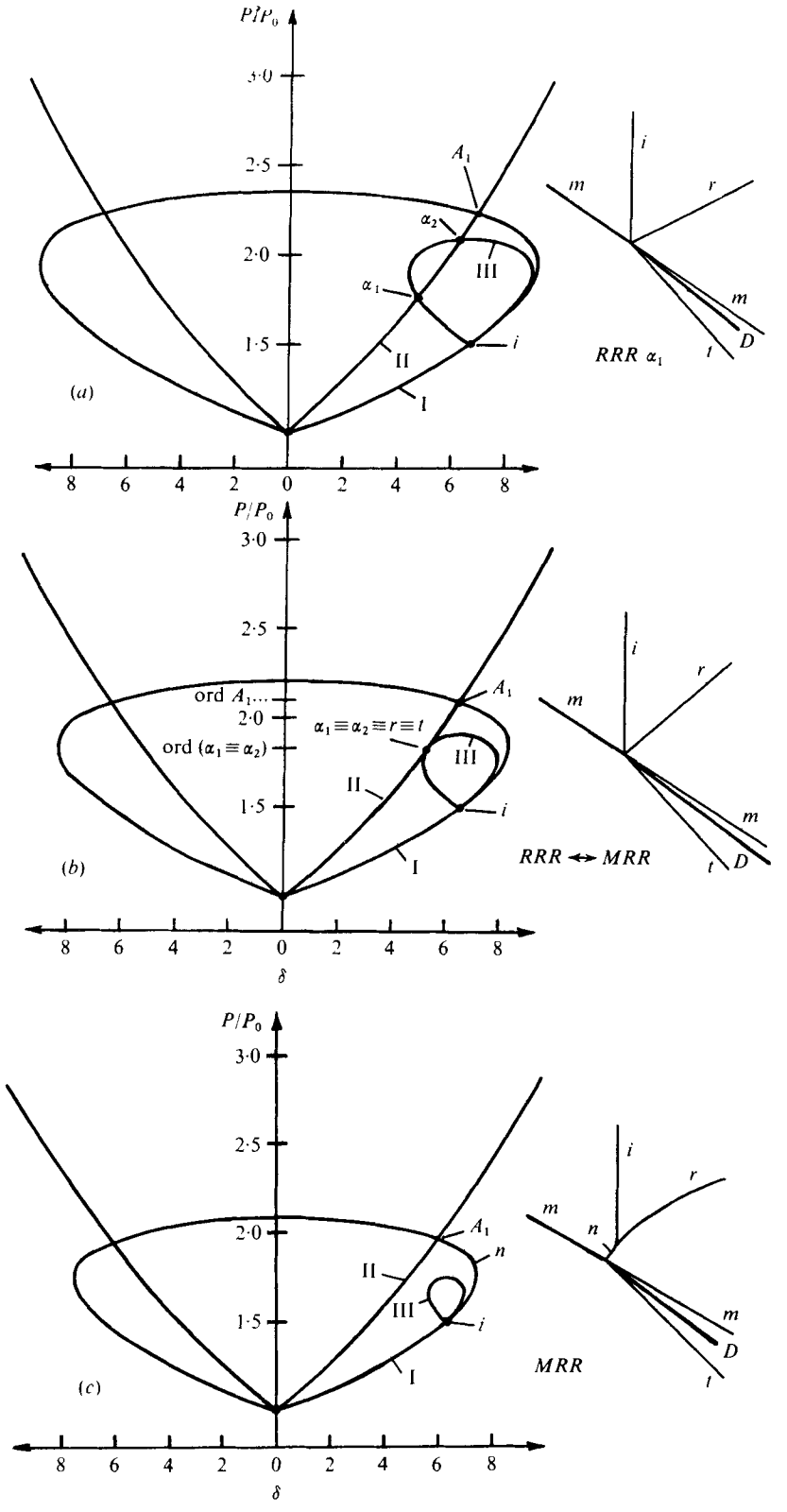

FIGURE 5. For legend see facing page.

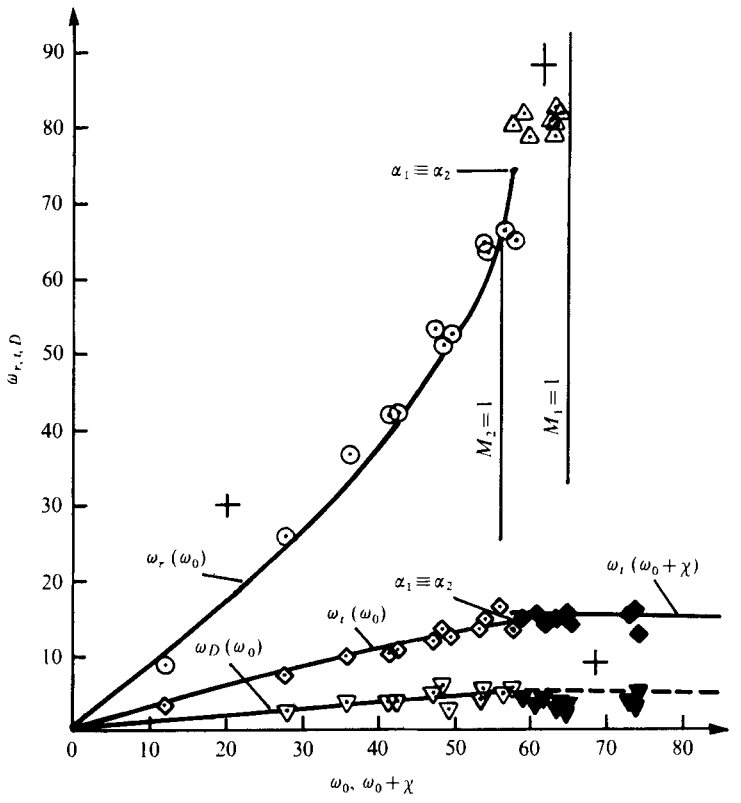

FIGURE 6. Comparison of the theoretically and experimentally determined wave angles for the refraction of a plane shock in the weak incident shock group ($\xi_i = 0{\cdot}66$) at an He/CO_2 interface. ω_D, deflexion angle of the gas interface; χ, trajectory path angle of the confluence point of the Mach reflexion with respect to the undisturbed interface; △, *MRR* experimental data for the reflected shock; ▽, ▼, *RRR* and *MRR* experimental data respectively from the deflected interface; ◆, *MRR* experimental data for the transmitted shock. N.B. ω_0 is measured with respect to the undisturbed interface for *RRR*, but with respect to the trajectory path for *MRR*. For other symbols see captions to figures 1, 2 and 5.

4. The strong incident shock group

Limitations on the driving pressure in our shock tube made it difficult for us to get into the strong shock range with the He/CO_2 interface. We overcame this problem by using an air/SF_6 interface and He as the driver gas. A typical sequence is illustrated in figure 8 for ξ_i constant at $\xi_i = 0{\cdot}25$ ($\xi_i^{-1} = 4$). For $\omega_0 = 50°$ we again obtained an *RRR* system which represented the α_1 root (figure 8*a*). When ω_0 was increased to $\omega_0 = 52{\cdot}70°$ as in figure 8(*b*), a critical point was reached where $\alpha_1 \equiv A_1$. The double-root condition was attained at a larger ω_0 of 52·825° (figure 8*c*) and therefore

FIGURE 5. Polar diagrams for the refraction of a plane shock in the weak incident shock group ($\xi_i = 0{\cdot}66$) at an He/CO_2 interface. (*a*) *RRR* at $\omega_0 = 50°$. (*b*) Transition condition defined by $\alpha_1 \equiv \alpha_2$ for $RRR \leftrightarrow MRR$, at $\omega_0 = 57{\cdot}40°$. (*c*) An irregular Mach-reflexion type of refraction *MRR* with no visible contact discontinuity (vortex sheet) arising from the confluence point of the Mach reflexion. *n*, Mach-stem shock. For other symbols see captions to figures 1 and 2.

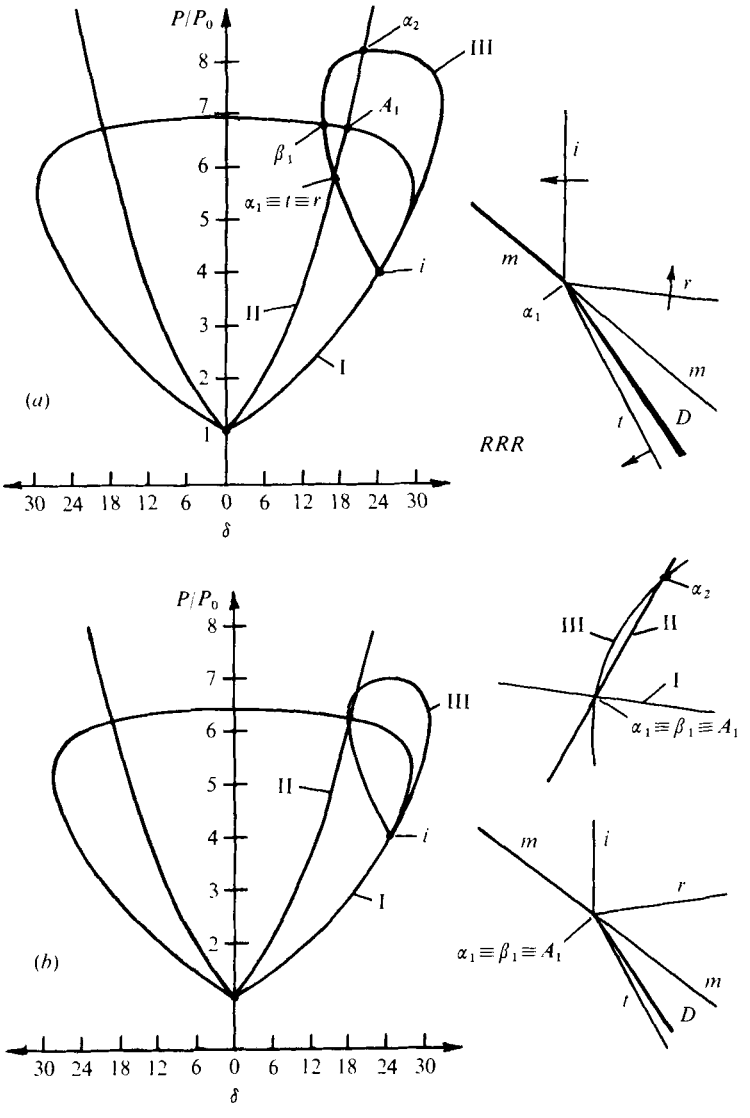

FIGURES 8 (*a*), (*b*). For legend see facing page.

ord $(\alpha_1 \equiv \alpha_2) >$ ord A_1 as required by the definition of a *strong* shock group. We did experiments with the objective of finding the transition condition to irregular refraction. Our results are shown in figure 9 and indicate that it takes place at $\alpha_1 \equiv A_1$ and certainly not at $\alpha_1 \equiv \alpha_2$. This conclusion is analogous to what Henderson & Lozzi found during their experiments on the reflexion of strong shocks, but now $\delta_n = \delta_t$.

After transition there is again an *MRR* system but with the difference that a vortex sheet is now visible (figure 10, plate 3; cf. figure 7). The theory of the wave confluence (triple) point as represented by the point β_1 (figure 8*d*) gives a unique solution for the wave angles ω_r and ω_{ni}. Similarly the theory at the point A_1 enables us to calculate the wave angles ω_t and ω_{nt} of the transmitted and Mach-stem shocks where they meet at

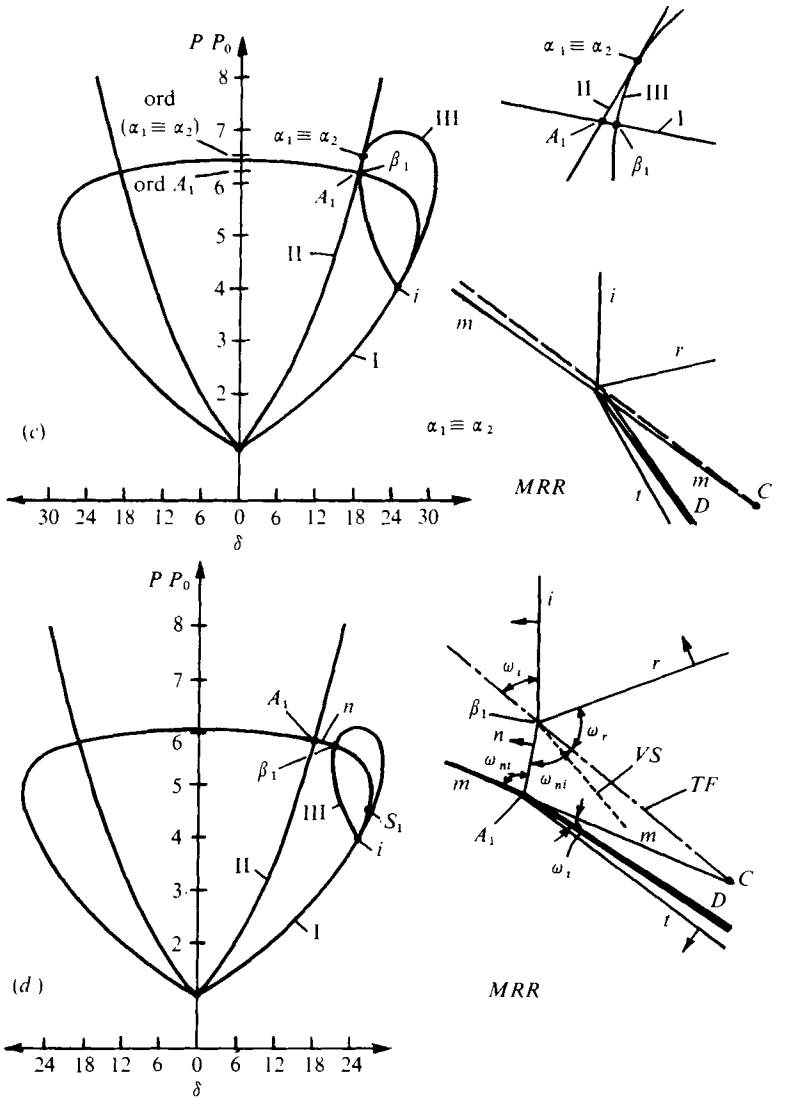

FIGURE 8. Polar diagrams for the refraction of a plane shock in the strong incident shock group ($\xi_i = 0{\cdot}25$) at an air/SF_6 interface. (*a*) *RRR* at $\omega_0 = 50{\cdot}00°$. (*b*) Transition condition defined by $\alpha_1 \equiv A_1 \equiv \beta_1$ for $RRR \leftrightarrow MRR$, at $\omega_0 = 52{\cdot}70°$. (*c*) *MRR* at $\alpha_1 \equiv \alpha_2$ when $\omega_0 = 52{\cdot}82_5°$ and where ord $(\alpha_1 \equiv \alpha_2) >$ ord A_1. (*d*) *MRR* for $\omega_0 = 55{\cdot}00°$; β_1, solution for the Mach-reflexion confluence point; ω_{ni}, ω_{nt}, wave angles of the Mach-stem shock on the Mach-reflexion confluence point and at the gas interface respectively. *C*, corner; *VS*, vortex sheet; *TP*, trajectory path. For other symbols see captions to figures 1, 2 and 5.

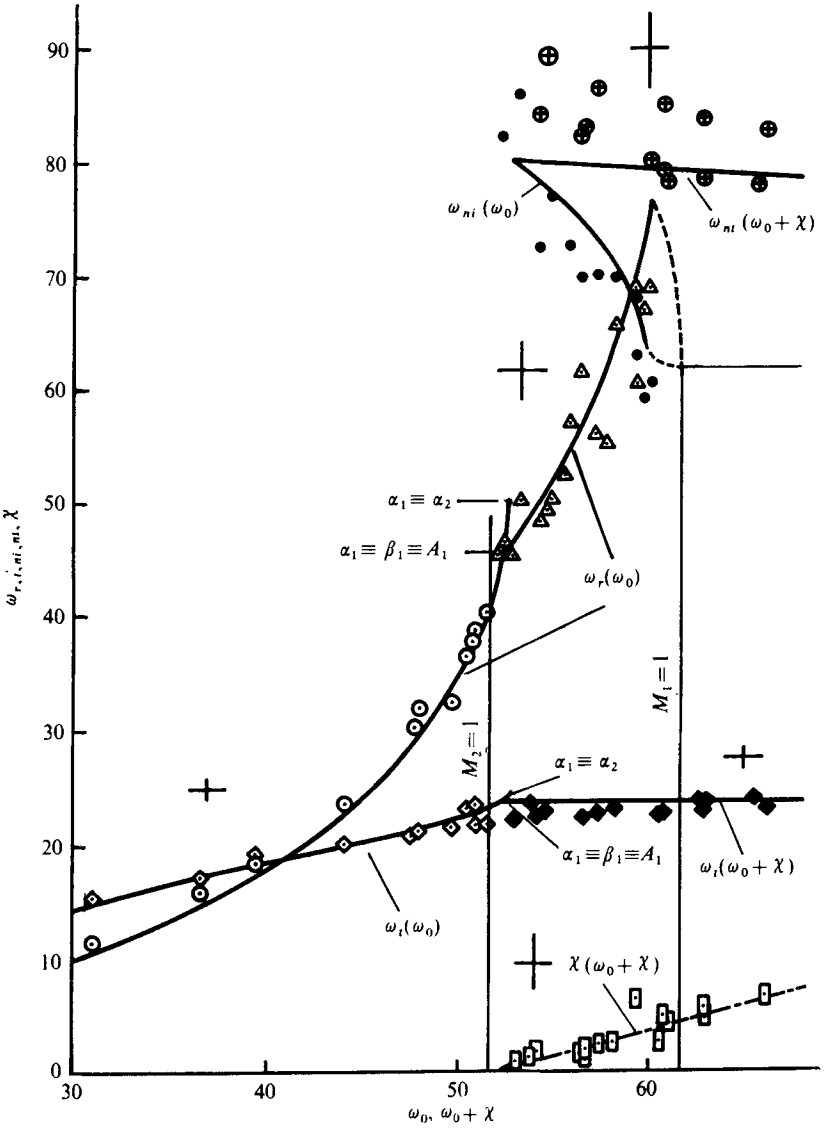

FIGURE 9. Comparison of theoretically and experimentally determined wave angles for the refraction of a plane shock in the strong incident shock group ($\xi_i = 0{\cdot}25$) at an air/SF_6 interface. ●, ω_{ni}, experimental data; ⊕, ω_{nt}, experimental data; ⊡, χ, experimental data; – – –, Guderley theory; — · — · —, χ, experimental curve. For other symbols see captions to figures 1, 2 and 5; see also the remark in the caption to figure 6.

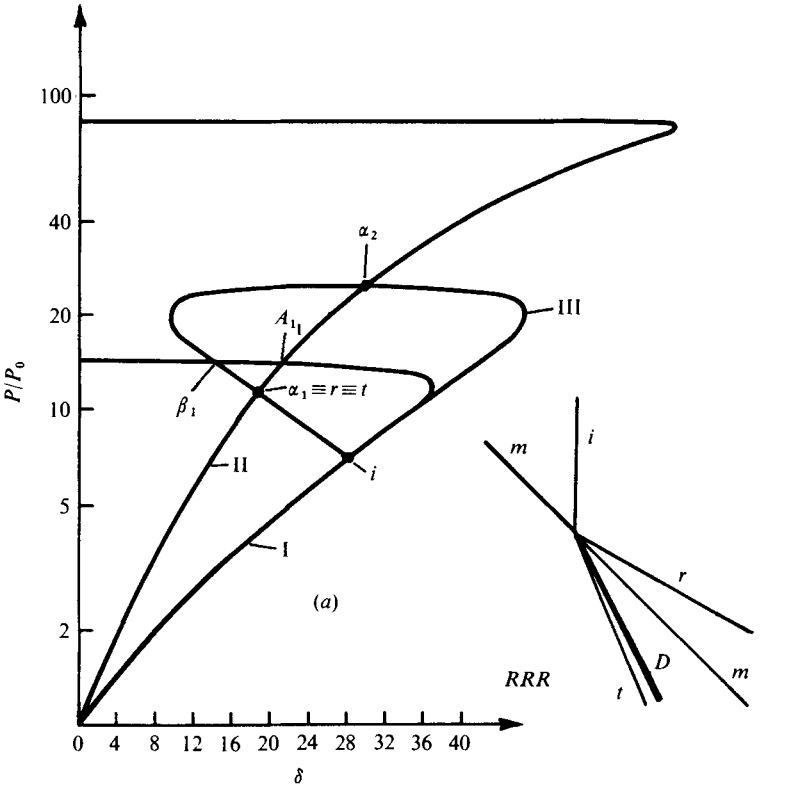

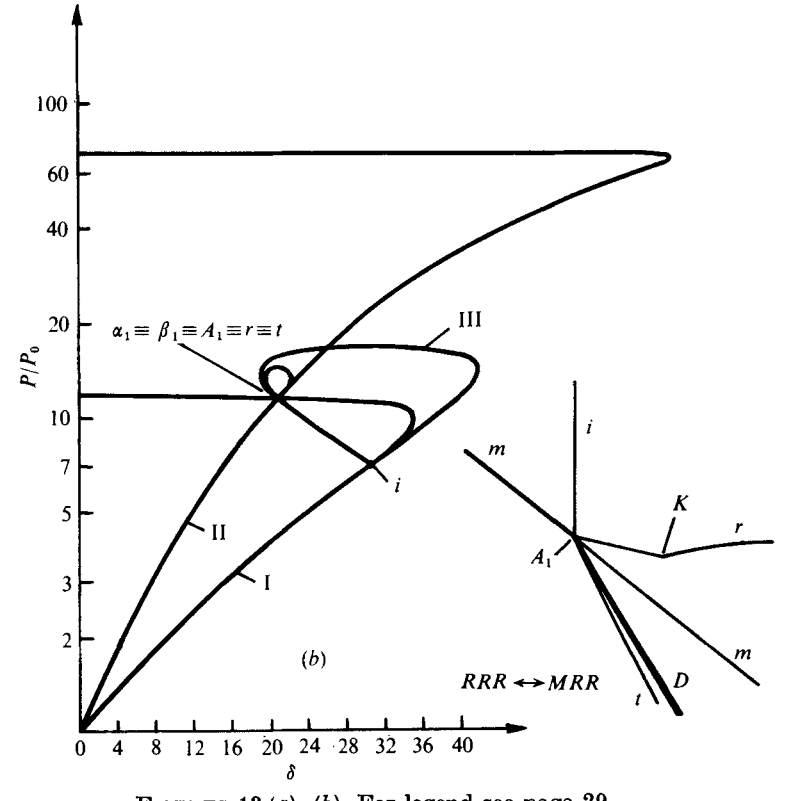

FIGURES 13 (*a*), (*b*). For legend see page 29.

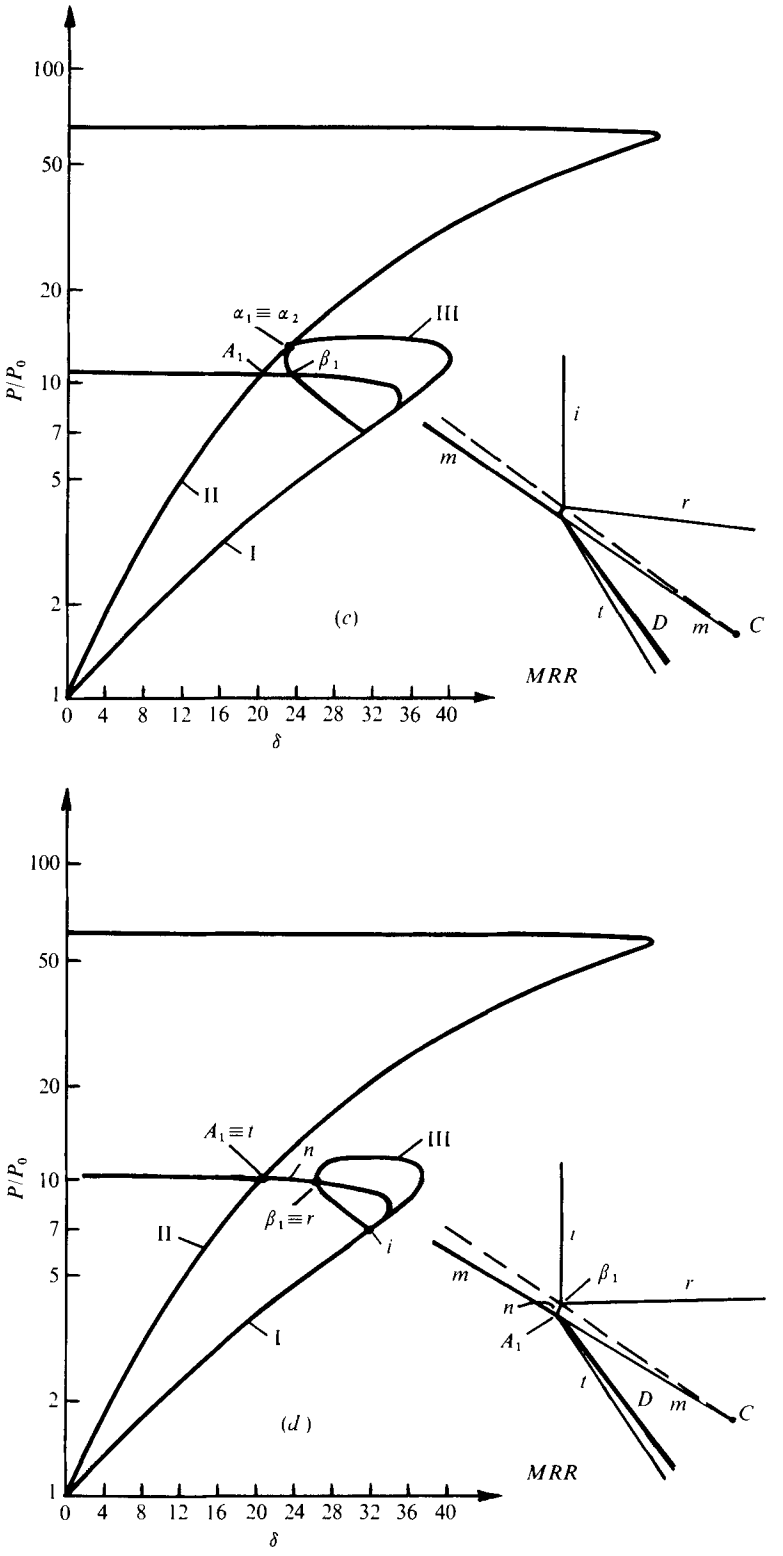

FIGURES 13 (*c*), (*d*). For legend see facing page.

the gas interface. The equation are given in Henderson (1966) and the results are compared with experiment in figure 9. The agreement is satisfactory for ω_r and ω_t for both the *RRR* and the *MRR* system. There are some discrepancies in ω_{ni} and ω_{nt} but we could not measure these wave angles as accurately as some of the others and mostly the theory is within the limits of experimental error. The polar theory terminates at an upper limit of $\omega_0 = 60{\cdot}0°$, where β_1 coincides with the sonic point S_1 ($\beta_1 \equiv S_1$). For ω_0 larger than this we used the Guderley (1962) theory, which gives results until ω_0 attains yet another limit $\omega_0 = 61{\cdot}76°$ such that $i \equiv S_1$, i.e. $M_1 = 1$. The Guderley theory agrees well with the ω_{ni} data but not with those for ω_r.

When $\omega_0 > 61{\cdot}76$, we have $M_1 < 1$ and the *MRR* system can no longer exist, so there must be a further transition to yet another irregular system, a photograph of which is shown in figure 11 (plate 3). To the best of our knowledge† it has not been previously reported. The incident and Mach-stem shocks i and n now appear as a continuous wave which is concave forwards along the segment formerly occupied by n. We shall call this system a concave-forwards irregular refraction *CFR*; we also found it in the weak shock series with $\xi_i = 0{\cdot}66°$ and $M_1 < 1$. The reflected shock r seems to have been dispersed into a band of weaker wavelets which nonetheless are still strong enough to induce vortex sheets in the flow. There also appears to be a reflected expansion wave propagating from the point where the incident shock strikes the interface, and the wave seems to be centred on this point. Furthermore there are two bands of cylindrical waves following the dispersed r wave and their origins seem to be in the mixing region between the two gases. One band appears to be generated before the mixing region encounters the back plate, while the other appears to arise from the deflected mixing region. At still larger ω_0 we reach a condition where the vortex sheets apparently vanish (figure 12, plate 3). This is analogous to the phenomenon shown in figure 7 and must be due to the smallness of the entropy gradient along and downstream of i.

5. The stronger incident shock group

Suppose now that ξ_i is decreased to $\xi_i = 0{\cdot}143$ ($\xi_i^{-1} = 7$). We then find for the air/SF_6 interface that there exists a small range of ω_0, namely $49{\cdot}3° < \omega_0 < 52{\cdot}3°$, for which the free-stream Mach number behind the reflected shock r is supersonic, i.e. $M_2 > 1$. This condition is well known from shock reflexion and diffraction experiments with rigid surfaces. It is found that r develops a sharp bend near the triple point, and if M_2 is sufficiently large then the change in the slope of r may sharpen into a discontinuity with an extra shock appearing in the flow. The system is sometimes called a double

† The analogous phenomenon in shock diffraction could have been observed by Fletcher, Taub & Bleakney (1951), had they taken schlieren photographs near glancing incidence, instead of interferograms.

FIGURE 13. Polar diagrams of the refraction of a plane shock in the stronger incident shock group ($\xi_i = 0{\cdot}143$) at an air/SF_6 interface. (*a*) *MMR* at $\omega_0 = 45{\cdot}00°$. (*b*) Transition condition defined by $\alpha_1 \equiv \beta_1 \equiv A_1$ at $\omega_0 = 50{\cdot}91°$ where $M_2 > 1$; notice the slope discontinuity in r. (*c*) *MRR* at $\alpha_1 \equiv \alpha_2$ when $\omega_0 = 53{\cdot}25°$. (*d*) *MRR* at $\omega_0 = 56°$. *K*, kink (slope discontinuity) in r. For other symbols see captions to figures 1, 2, 5 and 6.

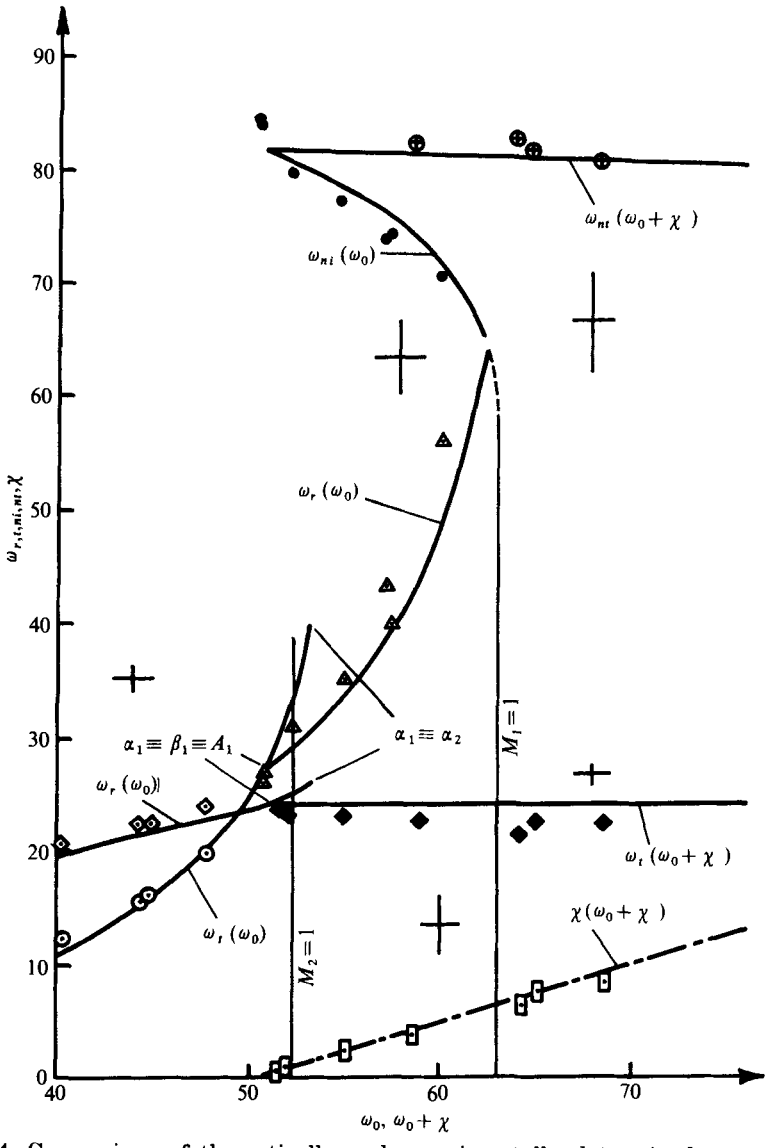

FIGURE 14. Comparison of theoretically and experimentally determined wave angles for the refraction of a plane shock wave in the stronger incident shock group ($\xi_i = 0{\cdot}143$) at an air/SF_6 interface. For symbols see caption to figure 9; see also the remark in the caption to figure 6.

Mach reflexion and it has been extensively studied (Gvosdeava *et al.* 1970; Semenov, Syshchikova & Berezkina 1970; Law & Glass 1971; Henderson & Lozzi 1975). According to the polar diagram in figure 13 it should also be present during refraction, although its existence in this case has not yet been reported. We did in fact obtain it, but the effect is too weak at $\xi_i = 7$ for it to show convincingly in any photograph we can reproduce here. Our experimental data are shown in figure 14 and agree rather better with the theory than the $\xi_i = 0{\cdot}25$ ($\xi_i^{-1} = 4$) data do, particularly the data for ω_{nt} and ω_{ni}. This is probably because the waves were stronger and sharper in the photographs and our angle measurements could be made a little more accurately. The transition

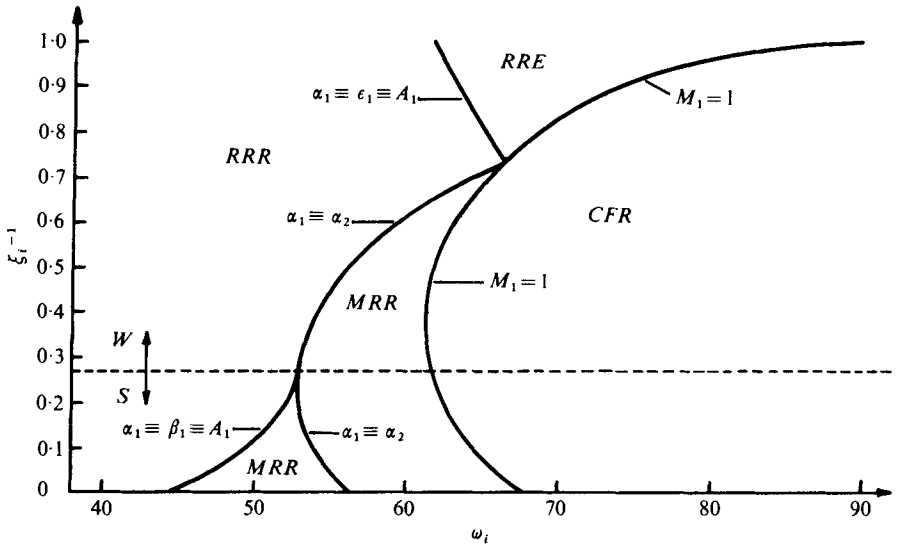

FIGURE 15. Map of the regions corresponding to the phenomena occurring on refraction of a plane shock wave at an air/SF_6 interface. *W*, weak shocks; *S*, strong shocks.

condition between the regular and the double-Mach-reflexion type of refraction was at $\alpha_1 \equiv A_1$ for $\omega_0 = 50{\cdot}91°$, and we again obtained a *CFR* system beyond the upper transition condition $i \equiv S_1$ for $\omega_0 = 63{\cdot}27°$.

Variations in the specific heats, particularly those for SF_6, are more likely to be of importance for this group than for any other: these effects are most pronounced when a shock is strongest and it then maps onto the subsonic part of its polar. In our case all the important points were on the supersonic part of the SF_6 polar and the effects of the gas imperfections were found to be less than the experimental error. Perfect-gas theory was therefore everywhere adequate for our purposes.

Finally we bring together all the transitional conditions and form a map which defines the circumstances in which each phenomenon exists; this is shown in figure 15.

6. Concluding remarks

Our studies of the polar diagram indicate that the wave systems described here probably constitute an exhaustive list of those for fast–slow refraction provided that the gases can be considered to be nearly perfect. In our experiments only SF_6 displayed appreciable variation in its specific heats and this caused only small changes in the wave angles and no changes in the wave-system structure. Of course the situation may be very different when imperfect-gas effects are large, as for example for very low density gases, or for hypersonic shock waves.

This work is supported by the Australian Research Grants Committee.

REFERENCES

ABD-EL-FATTAH, A. M., HENDERSON, L. F. & LOZZI, A. 1976 *J. Fluid Mech.* **76**, 157.

BLEAKNEY, W. & TAUB, A. H. 1959 *Rev. Mod. Phys.* **21**, 584.

FLETCHER, C. H., TAUB, A. H. & BLEAKNEY, W. 1951 *Rev. Mod. Phys.* **23**, 271.

GUDERLEY, K. G. 1962 *The Theory of Transonic Flow*. Pergamon.

GVOSDEAVA, L. G., BAZHENOVA, T. V., PREDVODITELEVA, O. H. & FOKEEV, V. P. 1970 *Astron. Acta* **15**, 503.

HENDERSON, L. F. 1966 *J. Fluid Mech.* **26**, 607.

HENDERSON, L. F. & LOZZI, A. 1975 *J. Fluid Mech.* **68**, 139.

JAHN, R. G. 1956 *J. Fluid Mech.* **1**, 457.

KAWAMURA, R. & SAITO, H. 1956 *J. Phys. Soc. Japan* **11**, 574.

LAW, C. K. & GLASS, I. I. 1971 *C.A.S.I. Trans.* **4**, 2.

LANDAU, L. D. & LIFSHITZ, E. M. 1959 *Fluid Mechanics*. Pergamon.

NEUMANN, J. VON 1943 Oblique reflexion of shock waves. In *Collected Works*, vol. 6, p. 238. Pergamon.

POLACHEK, H. & SEEGER, R. J. 1951 *Phys. Rev.* **84**, 992.

SEMENOV, A. H., SYSHCHIKOVA, M. P. & BEREZKINA, M. K. 1970 *Sov. Phys. Tech. Phys.* **15**, 795.

SMITH, L. C., 1945 *Office Sci. Res. Develop. Wash. Rep.* no. 6271.

TAUB, A. H. 1947 *Phys. Rev.* **72**, 51.

TAUB, A. H. 1951 *Phys. Rev.* **77**, 51.

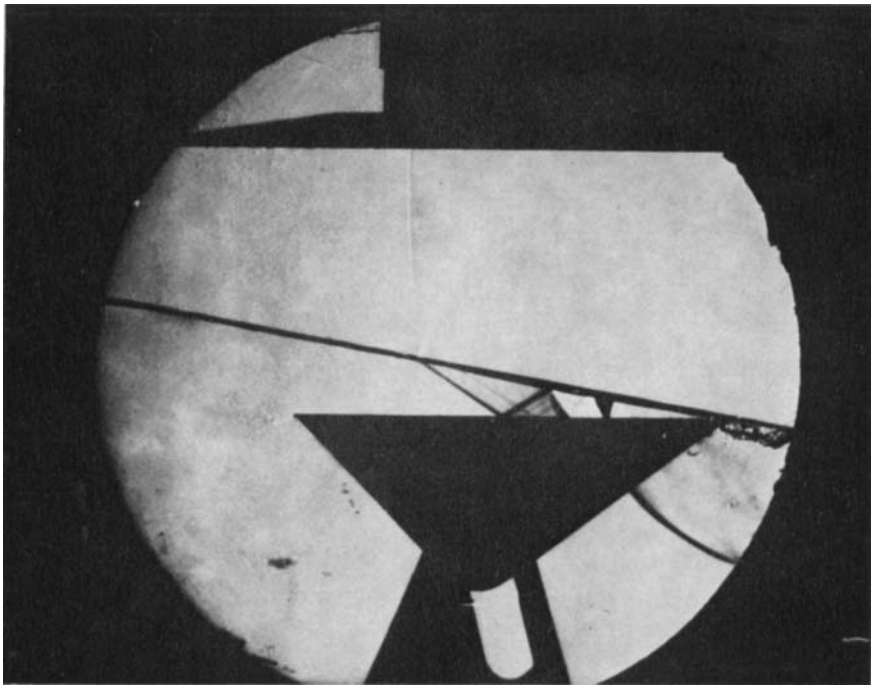

FIGURE 3. For legend see overleaf.

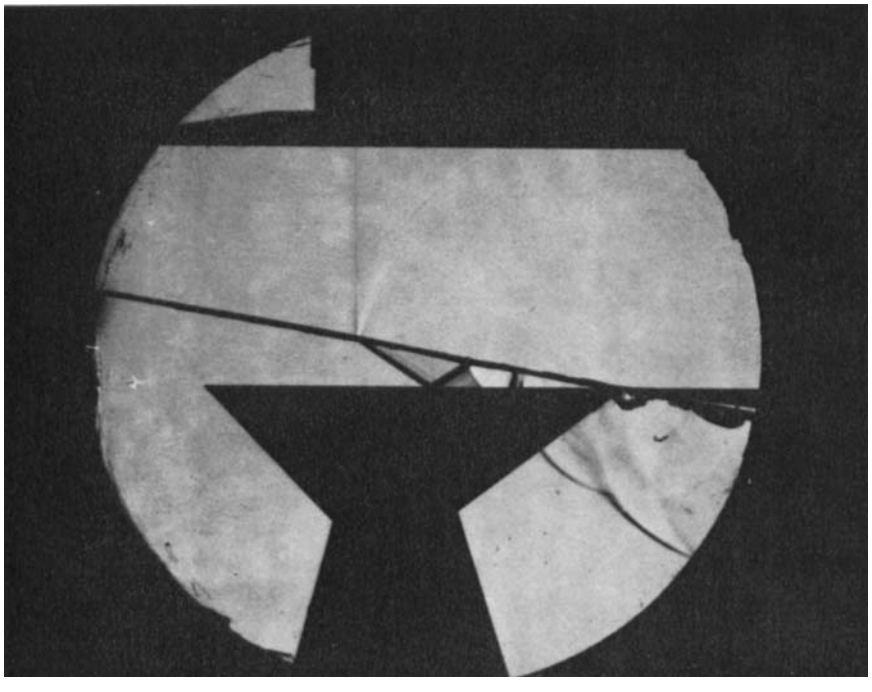

FIGURE 4. For legend see overleaf.

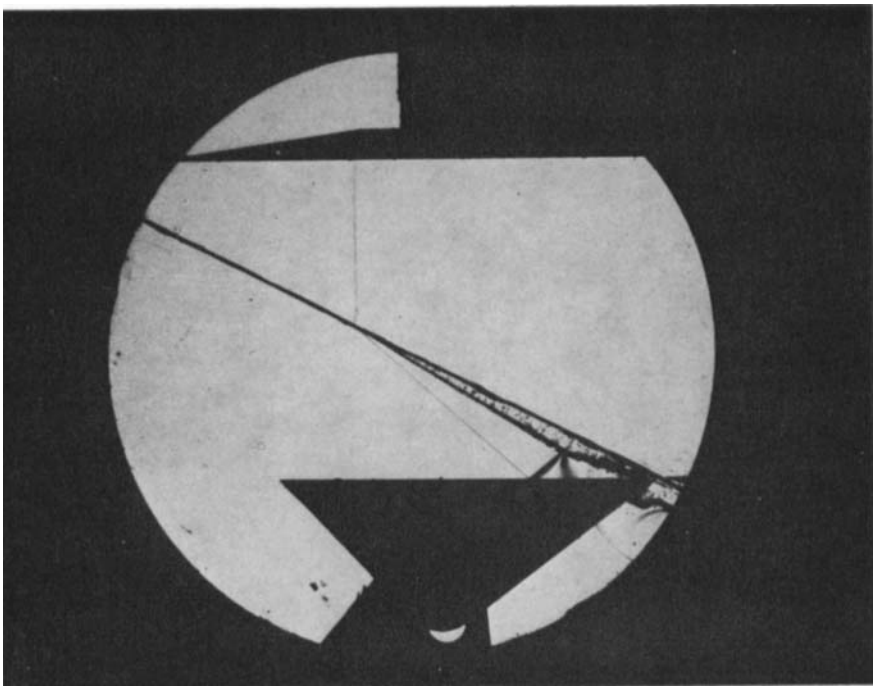

FIGURE 7. For legend see facing page.

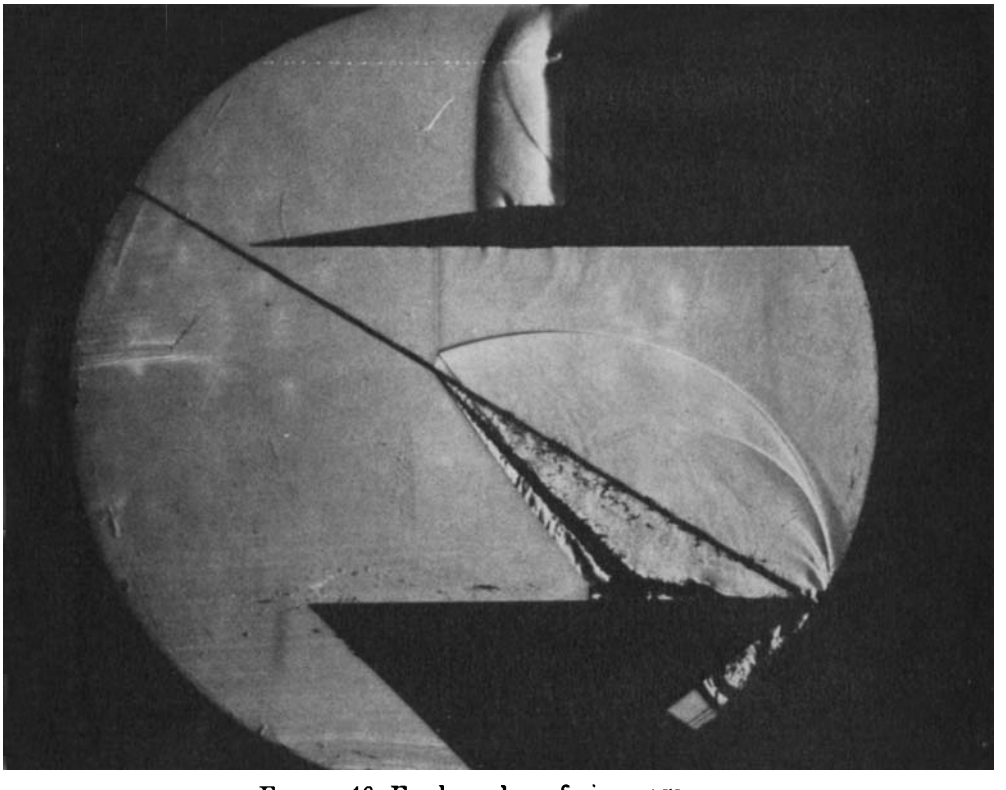

FIGURE 10. For legend see facing page.

FIGURE 3. Irregular refraction in the very weak ($\xi_i = 0{\cdot}909$) incident shock group at an air/SF_6 interface with $\omega_0 = 75{\cdot}20°$. The incident shock is curved and is believed to emit a continuous band of expansion waves but they are not visible. At the interface there is a reflected and centred expansion wave. The entire system is called an irregular centred expansion type of refraction *CER*. N.B. ω_0 is measured from the wire frame holding the membrane; if i was straight then ω_0 would be 79·8°.

FIGURE 4. Irregular refraction in the very weak ($\xi_i = 0{\cdot}909$) incident shock group at an air/SF_6 interface with $\omega_0 = 79{\cdot}0°$. The essential difference between this photograph and the one in figure 3 is the reduction in the gap width between the front and the back plates. As a result of this the incident shock is now straight. This is the true *CER* system.

FIGURE 7. Irregular Mach-reflexion type of refraction *MRR* in the weak ($\xi_i = 0{\cdot}66$) incident shock group at an He/CO_2 interface with $\omega_0 = 60{\cdot}7°$. The contact discontinuity (vortex sheet) is not visible in the Mach-reflexion part of the system as foreshadowed by von Neumann.

FIGURE 10. Irregular Mach-reflexion type of refraction *MRR* in the strong ($\xi_i = 0{\cdot}25$) incident shock group at an air/SF_6 interface with $\omega_0 = 55{\cdot}88°$. The contact discontinuity is visible in this photograph.

FIGURE 11. Irregular concave-forwards type of refraction *CFR* in the strong ($\xi_i = 0{\cdot}25$) incident shock group at an air/SF_6 interface with $\omega_0 = 59{\cdot}8°$. The reflected shock has apparently dispersed into a band of wavelets. Note the band of vortex sheets.

FIGURE 12. Irregular concave-forwards type of refraction *CFR* in the strong ($\xi_i = 0{\cdot}25$) incident shock group at an air/SF_6 interface with $\omega_0 = 60{\cdot}5°$. Compare with figure 11 and note that the vortex sheets have apparently vanished.

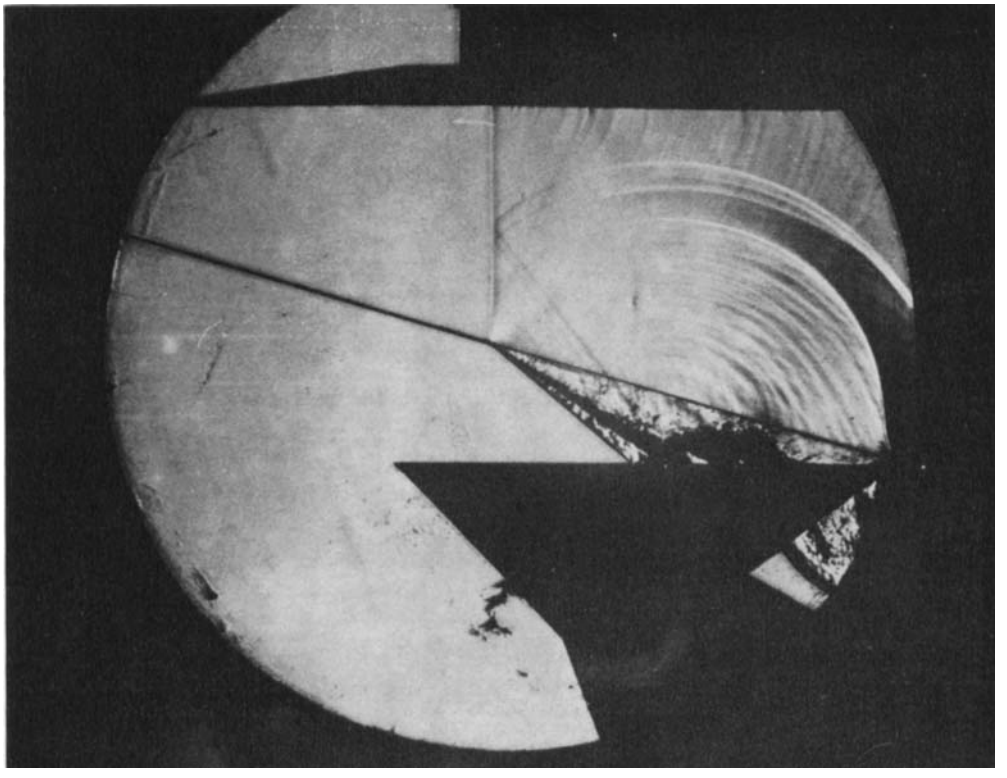

FIGURE 11. For legend see previous page.

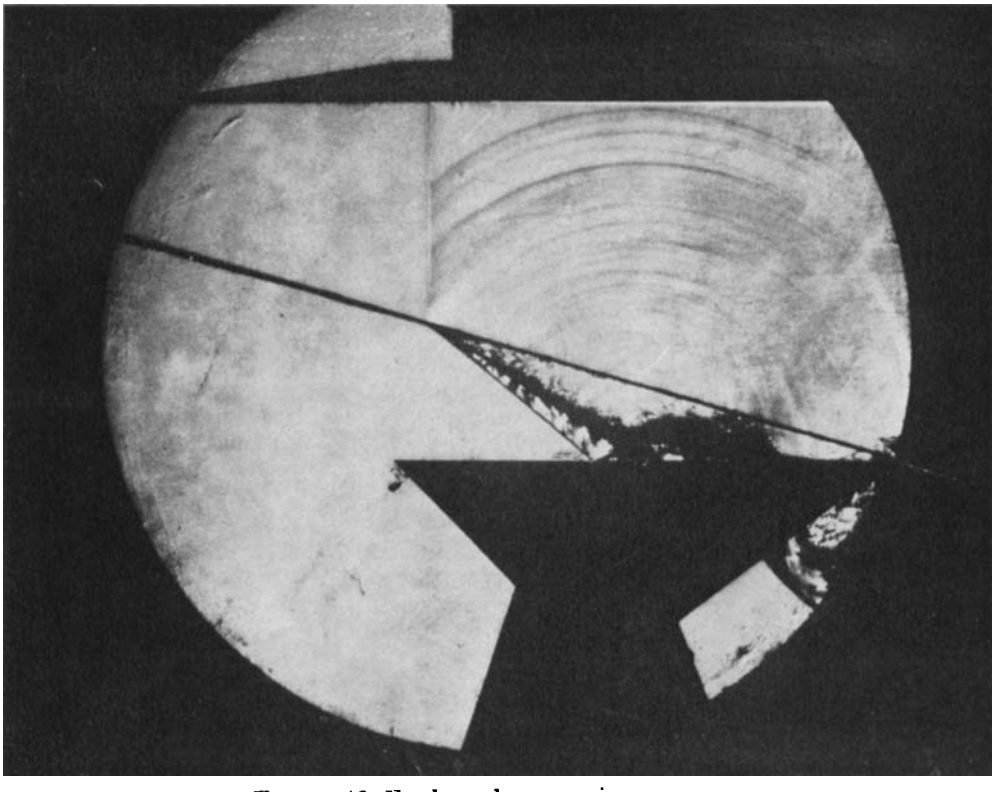

FIGURE 12. For legend see previous page.